
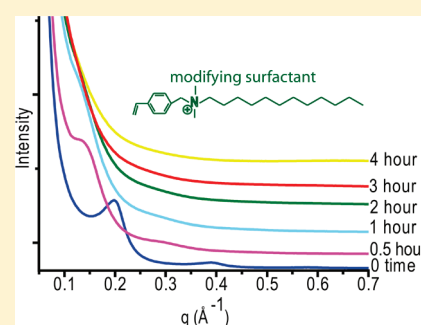


## Direct Observation of the Intergallery Expansion of Polystyrene–Montmorillonite Nanocomposites

Ranya Simons,<sup>†,‡</sup> Greg G. Qiao,<sup>\*,†</sup> Stuart A. Bateman,<sup>\*,‡</sup> Xiaoqing Zhang,<sup>§</sup> and Peter A. Lynch<sup>§</sup><sup>†</sup>Polymer Science Group, Department of Chemical and Biomolecular Engineering, University of Melbourne, Parkville, VIC, 3010, Australia<sup>‡</sup>Materials Science and Engineering, CSIRO, Graham Road, Highett VIC 3190, Australia<sup>§</sup>Materials Science and Engineering, CSIRO, Normanby Rd, Clayton VIC 3169, Australia Supporting Information

**ABSTRACT:** The intergallery expansion development of a series of differently modified montmorillonite polystyrene nanocomposites was directly observed with time-resolved in situ small-angle X-ray scattering (SAXS) using synchrotron radiation. The results indicated that the interlayer expansion varied depending on the clay modification and the chemical compatibility of the clay modifiers with the styrene monomer. The influence of the differently modified clays on the free radical polymerization was also investigated, particularly the effect on the conversion of styrene and molecular weight evolution of the polymer. On the basis of the kinetic study of the polymerization of styrene in the presence of varied modified clay particles, the intergallery expansion mechanism was postulated and discussed for different composite morphologies. Such studies provide an important guideline for the design of clay modifiers and development of clay–polymer nanocomposites.



**KEYWORDS:** SAXS, in situ polymerization, polystyrene, montmorillonite, kinetics, GC-MS, GPC, nanocomposites

## 1. INTRODUCTION

Polymer–clay nanocomposites have been widely investigated over the past decade, primarily because significant improvements in physical properties can be achieved at low clay concentrations.<sup>1</sup> These improvements and the resulting benefits on rheology and density have been captured commercially through the use of these materials in automobile components, packaging and construction materials.<sup>1,2</sup> The improvement in properties is largely dependent on the extent of the dispersion of the clay in the polymer matrix. Complete dispersion or “exfoliation” of layered clays such as montmorillonite (MMT) into individual clay platelets within the polymer matrix usually leads to the largest improvements in properties,<sup>3</sup> because of significantly enhanced interfacial interaction between the clay particles and the polymer. Intercalated nanocomposites occur when there is some interaction between the clay platelets and the polymer but it is insufficient to completely push the clay platelets apart, and the improvements in properties for these nanocomposites is usually only moderate. Microcomposites form when the interaction between the clay and the polymer is poor and the clay platelets remain in their tactoids or aggregates. The improvement in physical properties for these morphologies is low unless high levels of filler are added.

It is common to modify either the polymer to become more hydrophilic or the clay to become more organophilic in order to improve the compatibility of the clay and the polymer. Much work has focused on tailoring clay modifications for different polymer systems, however the driving force for exfoliation is still not completely understood.<sup>1</sup>

Recently we determined the effect of surfactant architecture on in situ polymerized polystyrene (PS)–MMT nanocomposites (Figure 1).<sup>4</sup> It was found that the architecture of the clay modifying surfactant was very important in determining the final morphology of the composite, and the important aspects that led to exfoliated structures included; the position of the cation in the surfactant, the inclusion of polymerizable groups that could react with styrene, the solubility of the surfactant in the monomer, and the length of the alkyl chain (i.e., size of the surfactant).<sup>4</sup>

Several studies have probed the intergallery expansion of nanocomposites through indirect or direct methods. Indirect observations of the dynamics of the surfactant layer in modified layered silicates during nanocomposite formation using electron paramagnetic resonance (EPR), provided insights into the behavior and influence of the clay modification on the composite.<sup>5–7</sup> Other investigations have attempted to study the morphological development of polymer–clay nanocomposites.<sup>8–14</sup> Giannelis et al.<sup>8,9</sup> investigated the intercalation kinetics of a polystyrene melt blended with montmorillonite using X-ray diffraction (XRD) and small-angle neutron scattering (SANS) and related the expansion of the clay layers with the motion of the polymer chains and the temperature of the melt blending. Chen et al.<sup>12</sup> utilized time-resolved XRD to track changes in *d*-spacing of epoxy-montmorillonite systems that led to intercalated

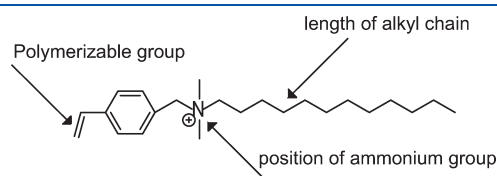
Received: August 31, 2010

Revised: March 31, 2011

Published: April 13, 2011

structures. Time dependent small-angle X-ray scattering (SAXS) was used for an epoxy-clay system at higher temperatures and used to track the disappearance of the diffractable peak over time as the clay became exfoliated.<sup>13</sup> In situ SAXS was used to track the crystallinity of PEO/MMT systems as the temperature varied.<sup>14</sup> Although investigations into the morphology development over cure time for epoxy-clay systems has been determined in the past,<sup>12,13,15</sup> there have been no investigations into the intergallery expansion mechanism and kinetics of in situ free-radical polymerized thermoplastic polymer systems, and this work will provide direct observation of the intergallery expansion and the effect of surface modification on the morphology development.

In this study, the morphological development and kinetics of a series of in situ polymerized polystyrene-montmorillonite nanocomposites was investigated in order to better understand the exfoliation mechanism that drives the final morphology of composites. For the first time, time-resolved in situ small-angle X-ray scattering (SAXS) was used to track the basal spacing of a series of modified and unmodified clays in styrene over its free-radical polymerization reaction period. The molecular weight evolution and the conversion of monomer of the styrene-clay solutions were also observed over the reaction period. The final polymerized composites were characterized using gel permeation chromatography (GPC) and solid-state NMR to probe the effect of the clay modification on the final composites. Intergallery expansion mechanisms for the development of different composite morphologies were also discussed for systems using differently modified clays.



**Figure 1.** Essential aspects of surfactant design for polystyrene–montmorillonite nanocomposites.<sup>4</sup>

## 2. EXPERIMENTAL SECTION

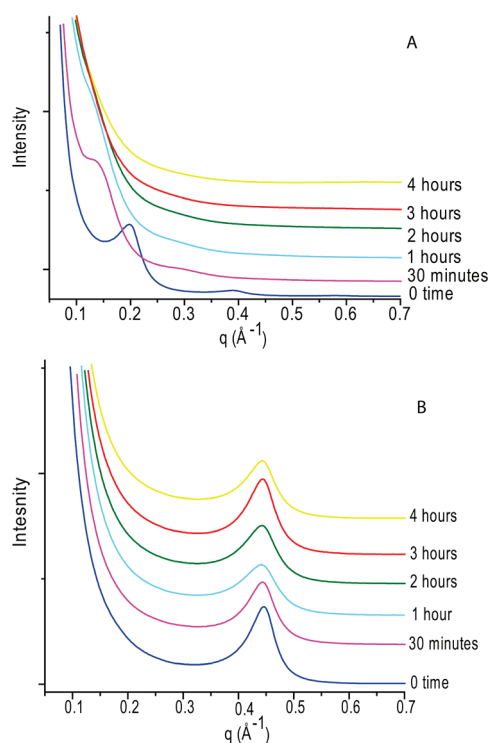
**2.1. Materials.** Styrene (99%) was purchased from Sigma-Aldrich and purified by passing through a basic alumina column. Lithium Chloride (LiCl, 98%) and diphenyl ether (DPE, 99%) was purchased from Sigma-Aldrich and used without further purification. The initiator 2,2-azobis(2-methylpropionitrile) (AIBN) (DuPont Australia Vazo 64) was recrystallized from ethanol and stored below 4 °C prior to use. Sodium montmorillonite (Na-MMT) was obtained from Southern Clay Products and had a cation exchange capacity (CEC) of 92 meq/100 g clay. The modified clays A-MMT, 12H-MMT, 12T-MMT, and EB-MMT were synthesized as detailed previously,<sup>4</sup> and the structures and properties of the modified clays are shown in Table 1.

**2.2. Sample Preparation.** Purified styrene monomer was deoxygenated by bubbling with argon for 1 h and then mixed with 5% wt of the modified and unmodified montmorillonite clays under vortex for 1 h. For the SAXS measurements, 0.5% wt AIBN was added, the solution deoxygenated by bubbling at 0 °C for another 30 min and then transferred into quartz capillaries and sealed under argon and kept at −86 °C until required. For the time-resolved conversion and molecular weight measurements, 5% wt DPE as internal standard was added to the styrene/clay mixtures, as well as 0.5% wt AIBN. To avoid sampling errors due to the high viscosity of the solutions, particularly at higher conversion, 1 mL samples of the styrene–clay–AIBN–DPE solutions were packed into glass ampules under argon and flame-sealed to exclude oxygen and stored at −86 °C until required. A separate ampule was used for each time measured. Completely polymerized solutions of the clays Na-MMT, A-MMT, 12H-MMT, 12T-MMT, and EB-MMT were obtained by heating at 80 °C for 48 h, and are termed Na-MMT-PS, A-MMT-PS, 12H-MMT-PS, 12T-MMT-PS, and EB-MMT-PS, respectively.

**2.3. Characterization.** SAXS was undertaken on the beamline at the Australian Synchrotron, Victoria, Australia at an energy of 12 KeV, for  $q$  values between 0.015 and 0.7 Å<sup>−1</sup>. For the in situ studies, styrene–clay solutions were contained and sealed in 1.5 mm diameter quartz capillaries. The solutions were measured simultaneously, with a styrene–AIBN solution containing no clay included as a control. Temperature control was achieved using a Lakeshore model 340 temperature control unit set at 80 °C. The measurements were taken on two areas of each capillary every minute for 4 h. The entire

**Table 1.** Properties of Unmodified and Modified Clay (reprinted with permission from ref ; copyright 2010 American Chemical Society)

Modified Clay	Modifying surfactant	d-spacing of clay Å	Solubility of surfactant in styrene	% surfactant exchanged (relative to cation exchange capacity (CEC))
Na-MMT	No surfactant (Sodium ion)	11.7	-	-
A-MMT		15.7	partial	71
12T-MMT		14.3	partial	69
12H-MMT		18.8	complete	82
EB-MMT		18.3	complete	79



**Figure 2.** SAXS spectra at selected styrene-polymerization times for (A) 12H-MMT and (B) 12T-MMT systems at 80 °C.

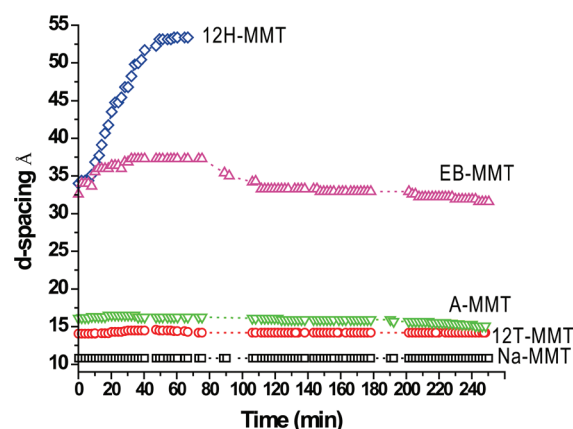
experiment was run twice for reproducibility and the results were reproducible to  $\pm 3\%$ . Scattering data was calibrated for background scattering and normalized to the primary beam intensity. The  $d$ -spacing of the clay at different times was calculated at the  $q$  value ( $\text{\AA}^{-1}$ ) corresponding to the diffraction peak maxima.

**Gel Permeation Chromatography.** (GPC) was performed on a Shimadzu system with a Wyatt DAWN DSP multiangle laser light scattering detector (690 nm, 30 mW) and a Wyatt OPTILAB EOS interferometric refractometer (690 nm). THF was used as the eluent with three Phenomenex phenogel columns (500,  $1 \times 10^4$ , and  $1 \times 10^6$  Å porosity) operated at 1 mL/min with the column temperature set at 30 °C. Astra software (Wyatt Technology Corp.) was used to process the data using known  $dn/dc$  values to determine the molecular weight.

To determine the molecular weight of the polystyrene chains attached to the clay, fully polymerized PS composites (cured for 48 h at 80 °C) were dissolved in THF, centrifuged, and washed repeatedly with THF until the supernatant was clear and the sediment was MMT with grafted PS. A reverse ion exchange was performed on the PS grafted montmorillonite to obtain the grafted PS chains;<sup>16</sup> the PS-grafted montmorillonite (0.3 g) and LiCl (0.3 g) were mixed in 240 mL of THF and refluxed at 70 °C for 48 h. The reaction was stopped, the polymer precipitated in methanol and dried, and the molecular weight determined via GPC. Thermal gravimetric analysis (TGA) of the resultant clay indicated that the reverse ion exchange had removed around 70% of the attached PS chains.

**Gas Chromatography–Mass Spectroscopy.** (GC-MS) was performed on a Shimadzu GC-17A gas chromatograph coupled to a GC-MS-QP 500 electron ionization mass spectrometer. DPE was used as an internal standard (5% wt styrene).

**High-Resolution Solid-State NMR.** experiments were conducted at room temperature using a Varian 300 NMR System at resonance frequencies of 75 MHz for  $^{13}\text{C}$  and 300 MHz for  $^1\text{H}$ .  $^{13}\text{C}$  NMR spectra were observed under cross-polarization, magic angle spinning (CP/MAS) and high power dipolar decoupling conditions. The 90° pulse was



**Figure 3.**  $d$ -spacing evolution of major  $d_{001}$  peak over the polymerization time for styrene/clay (5% wt) systems at 80 °C as obtained by SAXS.

5.5  $\mu\text{s}$  for  $^1\text{H}$  and  $^{13}\text{C}$  while the spinning rate of MAS was set at a value in the range of  $\sim 8$  kHz. A contact time of 1.0 ms was used for measuring CP/MAS spectra. The chemical shift of  $^{13}\text{C}$  CP/MAS spectra was determined by taking the carbonyl carbon of solid glycine (176.03 ppm) as an external reference standard.  $^1\text{H}$  spin–lattice relaxation ( $T_1$ ) data of the samples were measured indirectly through the change of  $^{13}\text{C}$  magnetization prepared by CP after the inversion–recovery pulse sequence in  $^1\text{H}$  channel.<sup>17</sup> Data analysis were conducted using the IGOR program from Wave Metrics Inc.

**Dynamic Light Scattering.** DLS measurements were performed on dilute samples of polystyrene–clay composites in THF, using a Malvern HPPS particle sizer with a 3.0 mW He–Ne laser operated at 633 nm. Analysis was performed at an angle of 173° and a constant temperature of 25 °C.

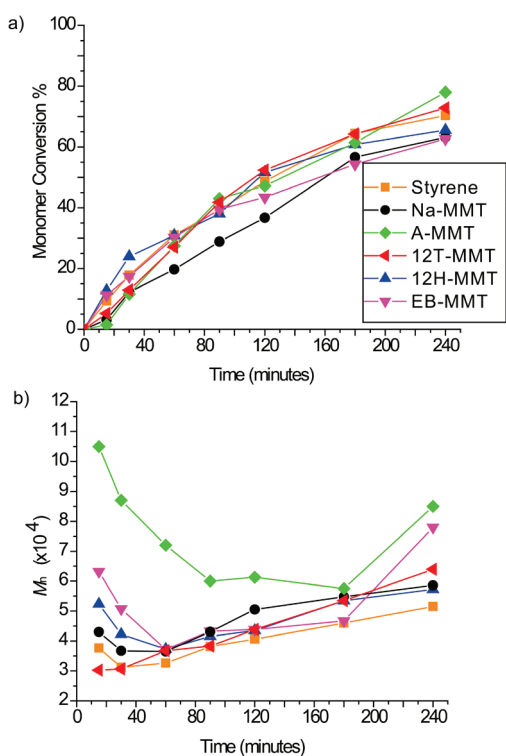
### 3. RESULTS AND DISCUSSION

As described in Table 1, both 12H-MMT and 12T-MMT contained polymerizable groups attached to the clay surface, however from previous studies,<sup>4</sup> only 12H-MMT led to exfoliated structures. The difference between these two surfactants was the position of the ammonium group in either a head (12H) or tail (12T) position relative to the styrene group. On the other hand, 12H and EB were the only surfactants readily soluble in styrene and had the highest level of swelling in styrene prior to polymerization. The amount of surfactant exchanged onto the clay relative to the cation exchange capacity (CEC) was determined through TGA and the values are listed in Table 1.

**3.1. Clay Dispersion Behavior during Styrene Polymerization.** In situ SAXS measurements using synchrotron radiation enabled us to determine the change of  $d$ -spacing of differently modified clays in the styrene polymerization reactions up to  $\sim 400$  Å. The resolution advantages of using synchrotron radiation allowed us to develop an accurate kinetic profile of the changes in intergallery spacing over time. The  $d$ -spacing was calculated at the  $q$  ( $\text{\AA}^{-1}$ ) value where the primary diffractable peak maxima was observed.<sup>18</sup> Figure 2 shows the SAXS spectra at selected times over the styrene polymerization period monitored for 2 typical systems; 12H-MMT and 12T-MMT. The change in the  $d$ -spacing of all the differently modified clays in styrene over reaction time is shown in Figure 3.

The  $d$ -spacing of the modified clays all increased after swelling in styrene before polymerization (compared with data in





**Figure 4.** (a) Conversion of styrene (as determined by GC-MS) and (b) molecular weight evolution over time (as determined by GPC) of the styrene/AIBN/clay systems at 80 °C. Complete conversion was achieved after 48 h.

Table 1), suggesting styrene monomer was intercalated between the clay layers upon mixing with the clay. The largest increase in  $d$ -spacing was observed for 12H-MMT and EB-MMT, and these clay modifiers were both soluble in styrene (Table 1). When heat was applied and the polymerization of styrene commenced, the 12H-MMT styrene solution exhibited an intergallery expansion that was very rapid in the first hour with the  $d$ -spacing reaching 55 Å, after which time the intensity of the diffractable peak decreased and then was no longer detected (Figure 2A), indicating that most of the clay platelets were exfoliated in the styrene/polystyrene (PS) system with further increased distance between clay platelets as well as disordered clay orientation. In contrast, the SAXS pattern of the 12T-MMT/styrene system did not change significantly over the polymerization time (Figure 2B), suggesting no significant exfoliation development occurred during the polymerization process. For EB-MMT the  $d$ -spacing increased from 33 to 37.5 Å in the first 20 min, then plateaued for 20 min, but after this time it decreased gradually back to the original value. The A- and Na-MMT systems displayed a similar kinetic profile to that of 12T-MMT system, although the initial  $d$ -spacing values were varied, indicating weak interaction between the clay and the styrene in the systems, and that the effect derived from styrene polymerization was minimal.

**3.2. Clay Effects on Styrene Polymerization.** The clay may affect the free radical polymerization in a series of complex ways.<sup>19–21</sup> Natural MMT has been observed to catalyze free radical polymerization of styrene at elevated temperatures,<sup>20</sup> but under other situations, MMT may act as a radical trap, effectively inhibiting free radical polymerizations.<sup>23–25</sup> These effects have been attributed to the different behavior of the clay

**Table 2.** Molecular Weight Data of Bulk and Attached PS in the Clay Composites

sample	bulk PS		attached PS		wt % of attached PS
	$M_n$ (kDa)	PDI	$M_n$ (kDa)	PDI	
polystyrene	136	2.18			0
Na-MMT-PS	176	1.98			0
A-MMT-PS	254	2.82			0
12T-MMT-PS	188	2.95	750	1.27	2.6
12H-MMT-PS	247	2.78	540	2.13	13
EB-MMT-PS	275	3.3	520	1.17	12

on the platelet edges and in the intergallery lamellae.<sup>19</sup> Surface modification of clay also adds another factor to influence the free-radical polymerization.

To investigate the effect of the modifying surfactant on the free radical polymerization of styrene, we monitored the reaction progression *ex situ* to observe the conversion of monomer and the evolution of molecular weight over reaction time with results shown in Figure 4.

The polymerization of styrene in the Na-MMT system proceeded at a slightly slower rate than those of modified clays and styrene system without clay. The difference was minimal among the differently modified clay–styrene systems and pure styrene polymerization. This suggests that the effect of the clay on the rate of styrene polymerization was not significant in this study (with clay loadings of 5 wt %).

The different clay/styrene systems exhibited a similar trend for the molecular weight evolution over time; the molecular weight values were initially high, slowly dropping to a minimum value at around 1 h and then slowly increasing again. The styrene/AIBN solution had consistently lower molecular weights over time compared to those containing clay. A-MMT had the highest consistent molecular weights over reaction time, followed by EB-MMT. It should be noted that the values presented are for the bulk polystyrene only; the solutions were filtered prior to characterization, which led to the removal of clay particles and any PS attached to the clays modified with reactive groups (12H-MMT and 12T-MMT). Thus, the molecular weights of any PS chains attached to the clay are not included in the results shown in Figure 4b. The polydispersity of molecular weight over time for these systems is shown in Figure S1 in the Supporting Information.

These molecular weight profiles are typical for free radical polymerizations and most likely correspond to the decomposition of AIBN into radicals reaching a maximum in the first hour (hence lower molecular weight due to a higher number of propagating radicals) and then slowly decreasing over the remaining reaction time, leading to higher molecular weights as the reaction progresses.

The high molecular weight detected in clay–styrene systems is consistent with the effect of diffusion;<sup>17</sup> the higher viscosity of the reaction mixture due to the clay decreased the probability of termination by combination, which was further decreased if PS chains grow on opposite sides of a clay platelet. The clay may also act as a free-radical trap reducing the number of radicals available and hence increasing the molecular weight.<sup>19–21</sup>

A-MMT-styrene and EB-MMT-styrene displayed the highest molecular weights; in these systems, styrene monomer intercalated between the layers as observed in the SAXS (Figure 3)

and then polymerized. Polymerization in confined spaces (i.e., the small space between clay layers approximately 10–30 Å) has been observed to suppress bimolecular terminations, and this has been utilized intentionally in the past to control molecular weight and stereospecificity of polymers.<sup>22</sup> Because A-MMT and EB-MMT do not have reactive groups on the clay surface to anchor the PS chains to, these longer intergallery PS chains might also be dissolved and captured in the GPC measurement, hence the overall observed molecular weight distribution of these polymers was higher.

The final composites after 100% styrene conversion (taken after 48 h reaction time) were investigated to capture the molecular weight of the bulk PS as well as those attached to the clay using a reverse ion-exchange to separate the two PS populations. The molecular weights and polydispersities of both fractions are presented in Table 2, as well as the amount of the attached PS isolated. It should be noted that from thermal gravimetric measurements, the reverse ion exchange technique removed around 70% of the attached PS.

The molecular weight of the PS without clay was 136 kDa with a polydispersity of 2.18, as would be expected for an uncontrolled free radical polymerization. All the systems containing clay displayed higher molecular weights. Na-MMT-PS exhibited a higher molecular weight of 176 kDa, due to the increase in viscosity of the clay containing system, and this effect was enhanced when the clay was better dispersed.

The 12H-MMT and 12T-MMT PS composites both contained polymerizable surfactants on the clay surface and hence PS chains could grow from the modifiers on the clay surface. In both cases, besides an increase in the bulk PS molecular weight, the molecular weight of attached PS chains were further significantly increased (540 kDa for 12H-MMT and 750 kDa for 12T-MMT composites), although there was more attached PS in the 12H-MMT system (13%). The polydispersities were relatively high for the bulk and attached PS, indicating a wide distribution of polystyrene chain lengths. The significant increase in the molecular weight of attached PS has not been observed before; Samakande et al<sup>12</sup> found that for polystyrene composites made with acrylate modified clay, the chains attached and not attached to the clay had similar molecular weights, and concluded the rate of the polymerization was the same. The different results observed in our work may be due to an effect of the different clay modification, or different experimental methods.

For the 12T-MMT composite, the intercalated morphology formed a confined space between the clay galleries, and hence the molecular weights of these chains may increase because of the decrease in the probability of termination through combination reactions.<sup>22–24</sup> This confined space effect has been observed and exploited in the past to produce long living polymer radicals in mesoporous zeolites, as observed by ESR and in molecular weight analysis.<sup>23</sup> This might also occur in the initial polymerization stage of 12H-MMT-styrene system when the clay *d*-spacing was still low (reaching a maximum of 55 Å for the first hour). It is also possible that the modified clay could also act as a charge transfer agent,<sup>19–21</sup> resulting in an increased rate of styrene polymerization growing from the 12H surfactant. As mentioned before, the clays may act as a radical trap,<sup>21</sup> reducing the number of propagating chains and hence decreasing the termination reactions by combination (and hence increasing the molecular weight of the tethered chains). Another possibility is that the AIBN initiator may partition differently in the bulk and the intergallery regions based on the solubility of the AIBN in the

intergallery region and this will be surface modification dependent. Direct measurement of this partitioning is difficult; however, indirect observation of the AIBN partitioning in clay/dichloromethane systems was investigated using GC-MS, and it was observed that more AIBN entered the 12H-MMT galleries than the EB-MMT, and significantly less entered the 12T-MMT (see the Supporting Information, Table S1). This suggests that the partitioning of AIBN in differently modified clays may have an influence in the intergallery polymerization. Higher levels of AIBN in the intergallery space would suggest a higher polymerization rate but lower molecular weight of PS because of the increased number of radicals; however, the *M<sub>n</sub>* was observed to increase. Other than a special affinity of the surfactants for AIBN, entropically the AIBN would prefer the larger space outside the intercalated clay compared to the intergallery region. This may also be why higher molecular weights are observed for attached PS (less AIBN in intergallery regions leads to lower termination rates). We believe the dominant effect on the molecular weight is most likely the effect of the confined space.

Another consideration is that for 12T-MMT, 69% of the ion exchange sites were exchanged with surfactant, while the amount of 12H-MMT surfactant exchanged was 82% (Table 1). 12H-MMT thus contained more sites for PS to grow from the clay surface, which may account for the difference in attached PS levels. A further complication is that the unmodified exchange sites still contain sodium ions. These sodium ions are expected to remain hydrated to some level and may potentially cause a cationic polymerization of styrene as observed by Solomon et al, further complicating the polymerization.<sup>19–21</sup>

It was initially anticipated that there should be no attached PS on EB-MMT. However, after repeated washing and centrifuging and Soxhlet extraction, 12% PS was still attached to the clay. A reverse ion-exchange was also performed for this fraction, and the resulting molecular weight of the PS is included in Table 2. This observed attached PS may be due to the EB surfactant acting as a chain transfer agent: the alkyl hydrogen on a benzyl group is known to be able to be abstracted by a growing radical,<sup>25–28</sup> in this case, the polystyryl radical, and this forms a stable radical on the ethyl group of the EB surfactant (Figure 5). Growing polystyrene chains could therefore terminate on the EB radical through combination mechanisms, or styrene monomer could react with the EB radical (particularly in the earlier stages of the reaction when monomer concentration is high), effectively leading to PS chains attached to the clay surface with a high molecular weight (520 kDa, ~2 times of that of the bulk PS).

Dynamic light scattering (DLS) measurements of very dilute (0.006 mg/mL) 12H-MMT-attached-PS and EB-MMT-attached-PS solutions indicated a particle size of around 300–400 nm in both cases (Figure 6), compared to a size of 100–200 nm for unmodified Na-MMT in water. These DLS values are consistent with the hypothesis that polystyrene chains with molecular weight of around 500 kDa (Table 2) have attached to both 12H-MMT and EB-MMT.

**3.3. Solid-State NMR Relaxation Times of Modified Clay–PS Composites.** High-resolution solid-state NMR is a powerful technique used to study intermolecular interactions among different components in multicomponent systems. For polymer clay nanocomposites, the interaction of the polymer chains and clay platelets, as well as the dispersion of the clay can be explored through a series of measurements, particularly the examination of <sup>1</sup>H T<sub>1</sub> (proton spin–lattice relaxations).<sup>17,29–34</sup> This method has been applied in the past to polystyrene,<sup>34</sup> nylon<sup>26–29</sup> and

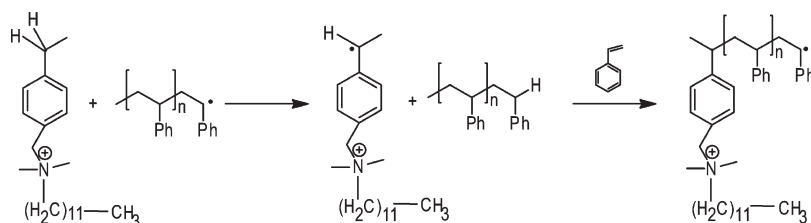


Figure 5. Proposed mechanism of hydrogen abstraction of surfactant EB by growing polystyryl radical.

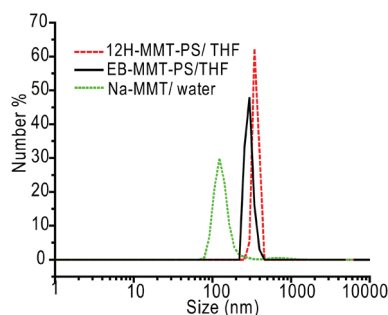


Figure 6. Dynamic light scattering (DLS) of dilute solutions of 12H-MMT and EB-MMT with attached PS in THF and Na-MMT in water.

starch-montmorillonite composite systems.<sup>17</sup> The benefit of this method is that the NMR measurement provides a bulk analysis methodology reflecting an average result from  $\sim 200$  mg of sample in the MAS rotor, rather than TEM and XRD methodologies, which have been widely used but only reflect a measurement area of around  $1 \mu\text{m}$ .

As described by VanderHart et al.,<sup>31–34</sup> naturally occurring montmorillonite clays normally contain 2–5% wt of paramagnetic  $\text{Fe}^{3+}$  ions. These ions have no effect on the embedded charge, but exert a sizable influence on the nuclear spin near the clay surface. Because one clay platelet is only 1 nm in thickness, the polymer chains directly interacting with the clay surface will be influenced by the  $\text{Fe}^{3+}$  ions. Through spin-diffusion interactions within the polymer matrix, a significant reduction in  $^1\text{H}$   $T_1$  data (measurement scale of  $\sim 30$  nm) occurs when such interaction is strong. Extremely strong interactions between  $\text{Fe}^{3+}$  ions in clay and polymer matrix could even cause signal weakening and line width broadening of the polymer chains (those directly attached on the surface of clay) and decrease their  $^1\text{H}$   $T_{1p}$  values (measurement scale of  $\sim 3$  nm).

The  $^{13}\text{C}$  CP/MAS spectra of all PS-clay composite samples (see Figure S2 in the Supporting Information) present similar line width as compared to that of pure PS, suggesting most of PS chains were not directly attached to the clay particles. The  $^1\text{H}$   $T_1$  data observed at 127 ppm (the main peak of benzene rings of PS) of these samples are listed in Table 3 (with raw data presented in the Supporting Information, Figure S3). The composites containing Na-MMT, A-MMT and 12T-MMT displayed similar  $^1\text{H}$   $T_1$  data to that of pure PS, which was consistent with the SAXS observations that the interaction between the clay platelets and the PS matrix was weak and the clay was not sufficiently well dispersed in the PS matrix in these systems. The 12T-MMT-PS contained only 2.6% attached PS (Table 2), which was below the detection limit of the solid-state NMR technique. In addition, the clay was not well dispersed in the PS matrix and hence there was no observable change in its  $^1\text{H}$   $T_1$ . However, the  $^1\text{H}$   $T_1$

Table 3. Solid-State NMR  $^1\text{H}$   $T_1$  Data of Clay–PS Composites

samples	$^1\text{H}$ $T_1$ (s) @ 127 ppm
PS–no clay	$2.6 \pm 0.2$
Na-MMT-PS	$2.7 \pm 0.2$
A-MMT-PS	$2.8 \pm 0.3$
12T-MMT-PS	$2.6 \pm 0.3$
12H-MMT-PS	$0.13 \pm 0.01$ (12%); $1.40 \pm 0.04$ (88%)
EB-MMT-PS	$0.18 \pm 0.01$ (13%); $1.7 \pm 0.4$ (87%)

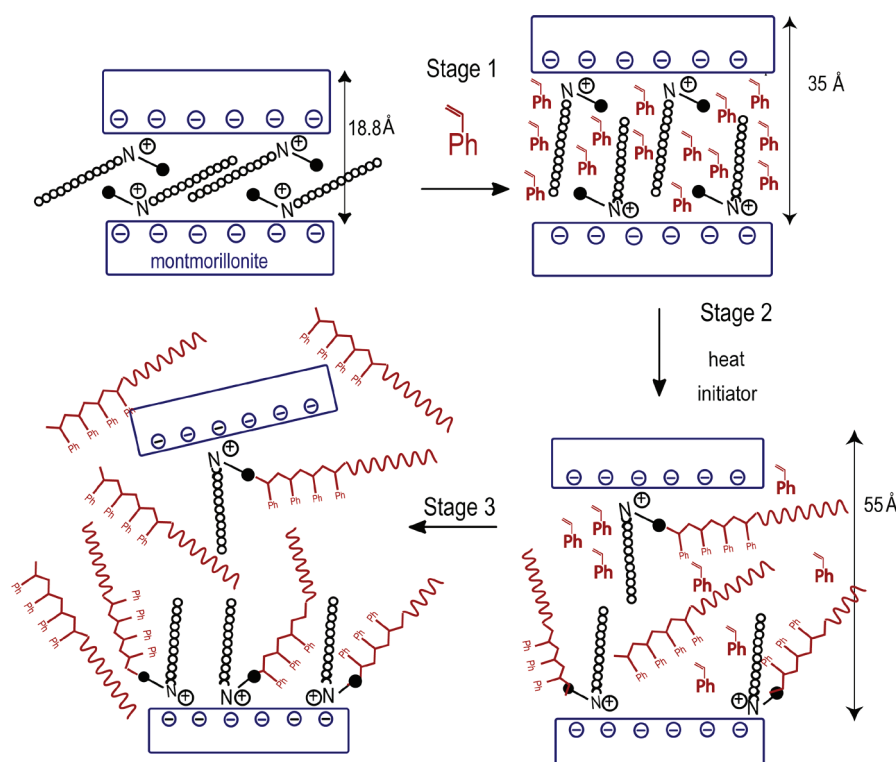
values of the systems containing 12H- and EB-MMT clays were significantly reduced (Table 3) as compared to that of pure PS. Such reduction in  $^1\text{H}$   $T_1$  was consistent with that reported previously for PS/clay systems,<sup>34</sup> and should be due to the effect of the paramagnetic  $\text{Fe}^{3+}$  ions in the clay, indicating significant interactions between the clay particles and PS matrix in these composites.

The lower the  $^1\text{H}$   $T_1$  values, the greater the interaction between the polymer and the clay, and the higher the level of exfoliation. The  $^1\text{H}$   $T_1$  for the PS composites containing 12H-MMT or EB-MMT displayed a fast initial decay and the overall decays seemed to fit well to a two-component-decay model, suggesting that the PS might experience different interaction levels with the clay, corresponding to different clay dispersion situations. The component with the lower value of  $^1\text{H}$   $T_1$  (0.13 or 0.18 s) could be related to the PS chains close to the clay (inside or just outside clay galleries including attached-PS, but no distinction between bound or not bounded PS), which have stronger interactions with clay particles. These short  $T_1$  values were also similar to those observed in exfoliated starch/clay nanocomposites where single  $T_1$  components were detected.<sup>17</sup> The component with  $T_1$  value of 1.4 or 1.7 s could mainly correspond to the PS chains having relatively weaker interactions with the clay (including bulk PS) in the two composites. Such nonexponential decay of  $^1\text{H}$   $T_1$  for these composites reflects the distribution variation of clay dispersion in the composites, rather than phase-separation in the PS matrix. A close comparison of the  $T_1$  data of 12H- and EB-MMT composites indicates more extensive clay dispersion occurred in 12H-MMT composite (lower  $T_1$  data), which is consistent with the SAXS observations.

**3.4. Intergallery Expansion Mechanism.** On the basis of the above results, intergallery expansion mechanisms were hypothesized for the differently modified clay composites and the mechanism for exfoliated morphologies is described in Figure 7.

Stage 1 of intergallery expansion occurred when the styrene and modified clay were mixed prior to styrene polymerization and heat. The  $d$ -spacing of the clay particles in this stage would depend on the swelling level of the clay in styrene monomers. The highest increase in  $d$ -spacing was observed for 12H-MMT





**Figure 7.** Proposed intergallery expansion mechanism for exfoliated structures (12H-MMT-PS). Key:  $\bullet = \text{Ph}$ ,  $\text{---} = (\text{CH}_2)_{11}\text{CH}_3$

and EB-MMT and corresponded to the  $d$ -spacing that would be expected if the alkyl chain portion of the surfactants adopted a near vertical orientation between the clay layers. The surfactants adopt this position to minimize energy because these surfactants are soluble in styrene.<sup>4</sup> Such an increase was also observed in other similar clay polymer systems.<sup>35,36</sup> The solubility of the modifier of A-MMT and 12T-MMT was poor in styrene, resulting in difficulty in its dispersion in styrene monomer and thus a lower  $d$ -spacing in stage 1. This first stage is important, because the higher the amount of styrene initially intercalated, the higher the level of intergallery polymerization that would occur in the composites.

During the initial stage of polymerization (stage 2), the styrene conversion was relatively low (<30%, Figure 4) and the solution viscosity was also low. The  $d$ -spacing could be further increased when monomers from the extragallery space were also involved in the polymerization of the monomer which was initially intercalated between the clay layers in stage 1, and the styrene group of the modifying surfactant on the clay surface. This could be the case in the 12H-MMT system, and the rapid increase in  $d$ -spacing in the first 60 min of the reaction to  $\sim 55$  Å suggests that styrene monomer from the extragallery space did participate in the polymerization between the clay layers, possibly due to the high solubility of the modifier of 12H-MMT in the styrene monomer, and its ability to polymerize with styrene. If there is stronger AIBN partitioning in the clay galleries of 12H-MMT, as suggested earlier, this could increase the number of radicals and hence increase the polymerization rate in the intergalleries, leading to increased expansion. After 60–120 min reaction, no observable diffraction was detected by SAXS, indicating the 12H-MMT clay layers continue to expand in a disordered fashion (and therefore not detectable by SAXS).

For intercalated nanocomposites such as EB-MMT and A-MMT, the increase in the  $d$ -spacing only occurred in the first 20 min, and only reached 37.5 and 16.6 Å, respectively. This lower  $d$ -spacing implies that it was mainly the styrene that was initially swollen into the clay layers in Stage 1 which was polymerized within the clay layers in the A-MMT and EB-MMT reactions, and that the rate of the intergallery polymerization was not higher than the rate of extragallery polymerization. Although the styrene also polymerized from the ethyl group on the EB surfactant through a hydrogen abstraction mechanism (Figure 5), the rate of this intergallery polymerization and the incidence of hydrogen abstraction was not sufficiently high enough to push the clay layers apart as rapidly as observed for the 12H-MMT system and thus the  $d$ -spacing value was not high.

For the 12T-MMT and Na-MMT styrene systems, the  $d$ -spacing change during this stage was minimal due to the low solubility of 12T in styrene, and hence the lower initial  $d$ -spacing (Stage 1). Growing polystyrene chains within the 12T-MMT layers may also react with more than one surfactant vinyl group on the 12T-MMT surface, effectively ‘pinning’ the clay layers, as has been observed in the past.<sup>37–39</sup> This may be more of a problem in the 12T-MMT than the 12H-MMT composites as the 12T styrene group is located further away from the exchange sites on the clay surface and hence is more accessible to other reactive groups.

After 60–80 min of the reaction, an increase in styrene conversion and a gradual increase in molecular weight caused the solution viscosities to increase, thus diffusion effects became more important during this stage (Stage 3). Further exfoliation development was only observed for the 12H-MMT composite (Figure 2A) as the clay platelets further disordered and became well dispersed in the matrix, corresponding to a disappearance of the diffractable peak. The formation of PS chains in the

intergallery polymerization would lead to greater separation and disorder of the platelets. This effect has been postulated for epoxy systems,<sup>40</sup> and is also supported by the molecular weight analysis of the fully polymerized PS composites (Table 2). The <sup>1</sup>H T<sub>1</sub> data from the solid state NMR suggests that there were two different populations of dispersed clay in the PS, and this suggests that while the system was exfoliated (as observed from SAXS), the clay did not achieve an homogeneous dispersion in the whole PS matrix.

For intercalated nanocomposites (EB-MMT, A-MMT, and 12T-MMT), a decrease in the *d*-spacing occurred during stage 3. The density of polystyrene (~1.05 g/cm<sup>3</sup>) is higher than the density of styrene monomer (~0.909 g/cm<sup>3</sup>), suggesting the polymerization of the styrene already located within the layers at Stage 1 would cause an increase in the density, thus the observed *d*-spacing would decrease as the conversion increased when no additional monomers moved into the intergalleries. This could be the case for these systems with poor swelling in styrene monomer and PS. For the Na-MMT system, no further intergallery expansion occurred in stage 3.

## CONCLUSIONS

The intergallery expansion development of a series of differently modified montmorillonite PS nanocomposites was directly observed using time-resolved in situ SAXS using Synchrotron radiation. Different clay modifications displayed minor differences in styrene polymerization rate and conversion, but longer PS chains were formed in intergallery spaces when the PS was attached to the clay surface. The results indicated that the compatibility of clay modifiers with the monomer and the presence of reactive polymerizable groups on the clay modifier were important to lead to high levels of clay exfoliation. Based on the kinetic study of the polymerization of styrene in the presence of varied modified clay particles, the intergallery expansion mechanism was postulated and discussed for different composite morphologies. Such studies provide an important guideline for the design of clay modifiers and development of clay–polymer nanocomposites.

## ASSOCIATED CONTENT

**S Supporting Information.** Additional table and figures (PDF). This material is available free of charge via the Internet at <http://pubs.acs.org>.

## AUTHOR INFORMATION

### Corresponding Author

\*E-mail: [gregghq@unimelb.edu.au](mailto:gregghq@unimelb.edu.au) (G.G.Q.); [Stuart.Bateman@csiro.au](mailto:Stuart.Bateman@csiro.au) (S.A.B.).

## ACKNOWLEDGMENT

The authors thank Nigel Kirby and Steven Mudie and the SAXS/WAXS beamline at the Australian Synchrotron, Victoria, Australia. The authors also thank Katherine Dean, Tor Kit Goh, and Jing Fung Tan for experimental contributions.

## REFERENCES

- (1) Chen, B. *Br. Ceram. Trans.* **2004**, *103* (6), 241–249.
- (2) Usuki; Kojima; Kawasumi; Okada; Fujushima; Kurauchi; Kamigaito *J. Mater. Res.* **1993**, *8* (5), 1179–84.
- (3) LeBaron, P. C.; Wang, Z.; Pinnavaia, T. J. *Appl. Clay Sci.* **1999**, *15* (1–2), 11–29.
- (4) Simons, R.; Qiao, G. G.; Powell, C. E.; Bateman, S. A. *Langmuir* **2010**, *26* (11), 9023–9031.
- (5) Panek, G.; Schleidt, S.; Mao, Q.; Wolkenhauer, M.; Spiess, H. W.; Jeschke, G. *Macromolecules* **2006**, *39* (6), 2191–2200.
- (6) Jeschke, G.; Panek, G.; Schleidt, S.; Jonas, U. *Polym. Eng. Sci.* **2004**, *44* (6), 1112–1121.
- (7) Schleidt, S.; Spiess, H.; Jeschke, G. *Colloid Polym. Sci.* **2006**, *284* (11), 1211–1219.
- (8) Vaia, R. A.; Jandt, K. D.; Kramer, E. J.; Giannelis, E. P. *Macromolecules* **1995**, *28* (24), 8080–8085.
- (9) Manias, E.; Chen, H.; Krishnamoorti, R.; Genzer, J.; Kramer, E. J.; Giannelis, E. P. *Macromolecules* **2000**, *33* (21), 7955–7966.
- (10) Meng, X.; Wang, Z.; Zhao, Z.; Du, X.; Bi, W.; Tang, T. *Polymer* **2007**, *48* (9), 2508–2519.
- (11) Meng, X.; Du, X.; Wang, Z.; Bi, W.; Tang, T. *Compos. Sci. Technol.* **2008**, *68* (7–8), 1815–1821.
- (12) Chen, J. h. S.; Poliks, M. D.; Ober, C. K.; Zhang, Y.; Wiesner, U.; Giannelis, E. *Polymer* **2002**, *43* (18), 4895–4904.
- (13) Chin, I. J.; Thurn-Albrecht, T.; Kim, H. C.; Russell, T. P.; Wang, J. *Polymer* **2001**, *42* (13), 5947–5952.
- (14) Sun, L.; Ertel, E. A.; Zhu, L.; Hsiao, B. S.; Avila-Orta, C. A.; Sics, I. *Langmuir* **2005**, *21* (13), 5672–5676.
- (15) Chen, C.; Khobaib, M.; Curliss, D. *Prog. Org. Coat.* **2003**, *47* (3–4), 376–383.
- (16) Samakande, A.; Hartmann, P. C.; Cloete, V.; Sanderson, R. D. *Polymer* **2007**, *48* (6), 1490–1499.
- (17) Zhang, X.; Dean, K.; Burgar, I. M. *Polym. J.* **2010**, *42* (8), 689–695.
- (18) Causin, V.; Marega, C.; Marigo, A.; Ferrara, G. *Polymer* **2005**, *46* (23), 9533–9537.
- (19) Solomon, D. H.; Loft, B. H. *J. Appl. Polym. Sci.* **1968**, *12*, 1253–1262.
- (20) Solomon, D. H.; Rosser, M. J. *J. Appl. Polym. Sci.* **1965**, *9*, 1261–1271.
- (21) Solomon, D. H.; Swift, J. D. *J. Appl. Polym. Sci.* **1967**, *11*, 2567–2575.
- (22) Satoh, K.; Kamigaito, M. *Chem. Rev.* **2009**, *109* (11), 5120–5156.
- (23) Ng, S. M.; Ogino, S.-i.; Aida, T.; Koyano, K. A.; Tatsumi, T. *Macromol. Rapid Commun.* **1997**, *18* (12), 991–996.
- (24) Allcock, H. R.; Ferrar, W. T.; Levin, M. L. *Macromolecules* **1982**, *15* (3), 697–703.
- (25) Bevington, J. C.; Cywar, D. A.; Huckerby, T. N.; Senogles, E.; Tirrell, D. A. *Eur. Polym. J.* **1990**, *26* (8), 871–875.
- (26) Bevington, J. C.; Cywar, D. A.; Huckerby, T. N.; Senogles, E.; Tirrell, D. A. *Eur. Polym. J.* **1990**, *26* (1), 41–46.
- (27) Mayo, F. R. *J. Am. Chem. Soc.* **1943**, *65* (12), 2324–2329.
- (28) McCormick, D. T.; Fordham, Z. W.; Smith, J.; McMullan, P. J.; Thames, S. F.; Allan Guymon, C. *Polymer* **2003**, *44* (9), 2751–2759.
- (29) Alfrey, T.; Bohrer, J.; Mark, H., *Copolymerisation*; Interscience: New York, 1952.
- (30) Bertmer, M.; Wang, M.; Krüger, M.; Blümich, B.; Litvinov, V. M.; van Es, M. *Chem. Mater.* **2007**, *19* (5), 1089–1097.
- (31) VanderHart, D. L.; Asano, A.; Gilman, J. W. *Chem. Mater.* **2001**, *13* (10), 3796–3809.
- (32) VanderHart, D. L.; Asano, A.; Gilman, J. W. *Chem. Mater.* **2001**, *13* (10), 3781–3795.
- (33) VanderHart, D. L.; Asano, A.; Gilman, J. W. *Macromolecules* **2001**, *34* (12), 3819–3822.
- (34) Bourbigot, S.; VanderHart, D. L.; Gilman, J. W.; Awad, W. H.; Davis, R. D.; Morgan, A. B.; Wilkie, C. A. *J. Polym. Sci., Part B: Polym. Phys.* **2003**, *41* (24), 3188–3213.
- (35) Usuki; Kawasumi; Kojima; Okada; Kurauchi *J. Mater. Res.* **1993**, *8* (5), 1174–8.



- (36) Lan, T.; Kaviratna, P.; Pinnavaia, T. *Chem. Mater.* **1995**, 7, 2144–50.
- (37) Zhang, J.; Jiang, D. D.; Wang, D.; Wilkie, C. A. *Polym. Degrad. Stab.* **2006**, 91 (11), 2665–2674.
- (38) Zhang, J.; Jiang, D. D.; Wilkie, C. A. *Polym. Degrad. Stab.* **2006**, 91 (4), 641–648.
- (39) Zhang, J.; Wilkie, C. A. *Polymer* **2006**, 47 (16), 5736–5743.
- (40) Lan, T.; Kaviratna, P.; Pinnavaia, T. *Chem. Mater.* **1995**, 7, 2144–50.